Int J Adv Manuf Technol (2017) 93:3419–3427
DOI 10.1007/s00170-017-0683-5

ORIGINAL ARTICLE

Experimental study on the cutting temperature of textured carbide tool embedded with graphite

Wenlong Song[1,2] · **Zuocheng Wang**[1] · **Shoujun Wang**[2] · **Ke Zhou**[2] · **Zongxin Guo**[2]

Received: 9 February 2017 / Accepted: 14 June 2017 / Published online: 18 July 2017

Abstract To enhance the anti-friction and anti-wear properties of the WC/TiC/Co carbide, micro-EDM was selected to fabricate textured micro-holes on the carbide surface, and graphite was embedded into the micro-holes to form self-lubricating tools. Dry machining tests on AISI 1045 hardened steel were carried out with the self-lubricating tool and conventional ones. The cutting temperature and tool wear were investigated and compared. The results showed that the self-lubricating tool embedded with graphite exhibited excellent efficiency and stability in reducing cutting temperature, and then the tool wear was reduced compared to that of the conventional one. Through the analysis of test results and cutting temperature distribution theory, the mechanisms responsible are put forward: the first one is the formation of a graphite film on the tool rake face, which is conducive to reducing the temperature of chip and tool caused by tool-chip friction and chip deformation; the other one is attributed to the reduced actual contact length at the tool-chip interface due to the micro-holes, which is propitious to lower the temperature of chip and tool caused by tool-chip friction, supply more graphite, and store chip debris.

✉ Zuocheng Wang
zcwang@sdu.edu.cn

Wenlong Song
wlsong1981@163.com

[1] Department of Material Science & Engineering, Shandong University, No. 17923 Jingshi Road, 250061 Jinan, Shandong Province, People's Republic of China

[2] Department of Mechanical Engineering, Jining University, Qufu 273155, People's Republic of China

Keywords Self-lubricating · Graphite · Cutting temperature · Tool wear

1 Introduction

Owing to high toughness and high wear resistance, cemented carbide (WC/TiC/Co) is the well-known and extensively used tool materials for industrial production. However, without the cooling and lubrication of cutting fluid, cemented carbide is characterized by the higher friction coefficient, dissatisfied resistance to friction and wear, and relatively low tool lives. To promote the cutting performance of cemented carbide in dry machining, considerable efforts have been made, for instance, optimum tool geometries and cutting conditions [1], the minimum quantity lubrication [1], heat treatment [2], cryogenic treatment [3, 4], coated tool such as hard coatings and soft coatings [5–15], and surface textures [16–28]. It is believed that it is promising to develop self-lubricating tools by forming the lubricating film at the tool-chip interface with combination of textures and solid lubricants.

Recently, surface texturing has been introduced to improve the anti-wear properties of contact surface and has been applied in many fields predominantly such as cutting tools, engine cylinder liners, and bearings [16–20]. The surface texturing is conducive to entrapping the wear debris, supplying lubricant by fluid reservoirs creation, and enhancing the load-bearing capacity by a hydrodynamic effect, which may effectively elevate wear resistance. For example, Lei et al. [20] fabricated micro-hole arrays on the tool rake face in order to facilitate lubrication and exhibited a 10–30% reduction in cutting force during machining harden steel processes. Sugihara et al. [21] reported a cutting tool with a nano/micro-textured surface by femtosecond laser technology, and the face-milling experiments in machining aluminum alloy processes

Table 1 Properties of the cemented carbide material

Composition	Density (g/cm^3)	Hardness (GPa)	Flexural strength (MPa)	Young' modulus (GPa)	Thermal expansion coefficient (10^{-6}/k)	Poisson's ratio
WC + TiC + Co	11.5	15.5	1130.0	510	6.51	0.25

exhibited that the textured surface improved anti-adhesive behavior on the tool rake face. Hu et al. [22] reported that a combination of surface texturing and hot pressed MoS_2 coatings on the steel surface was more effective in reducing friction coefficient and improving service life. Obikawa et al. [23] reported that it was more effective in reducing friction and wear with textures parallel to the cutting edge on the rake face compared with other kinds of textures. Deng et al. [24] fabricated micro-scale textures with different geometrical arrays on the tool rake face and filled MoS_2 solid lubricants into the textures. Results exhibited that the cutting performance of the textured tools was significantly improved compared to the conventional ones, and elliptical grooves were more effective than the parallel or perpendicular grooves. Then, they combined the textured tools with WS_2, WS_2/Zr, and nitride coatings to improve the tool cutting performance [25–28].

The reviewed literatures indicate that the textures filled with solid lubricants could form the lubricating film at the sliding interface in cutting and friction processes, which is beneficial to improve the anti-friction and anti-wear properties. However, the previous researches mainly concentrate on the sulfides such as MoS_2 and WS_2, and these sulfides are sensitive to higher temperature. As service temperature is above 450–550 °C, they begin to be oxidized and gradually lose the lubricating effect [10–19].

In comparison with the sulfides, graphite (C) is extensively applied in various fields of industrial production. It owns physical (i.e., it prevents adhesion), chemical (i.e., it enables tribo-chemical reactions), and microstructural (i.e., it owns a hexagonal lamellar structure with low shear strength) effects on the tribological contact of sliding surfaces. Graphite is usually made as solid lubricating additive in cutting fluid to decrease the cutting temperature and tool wear [19] and could serve excellently in a wider service temperature range. However, few literatures have studied on the cutting performance in cutting temperature of the tool combined with graphite and textures, and they need to be further studied.

In this study, micro-EDM was applied to prepare micro-holes with diameter of about 150 μm to supply more lubricants and entrap more chip debris on the tool-chip contact area, and then graphite were filled into these textured micro-holes to make self-lubricating tool (ST). Dry turning tests on AISI 1045 hardened steel were carried out with the ST tool and conventional one without micro-holes and graphite (CT). The cutting temperature and tool wear were measured and compared. Through the analysis of cutting temperature distribution theory and test results, the possible mechanisms of reduced cutting temperature and tool wear for the ST tool were studied.

2 Experimental procedures

2.1 Preparation of the test samples

Cemented carbide was used for preparation of the test material. The composition, physical, and mechanical properties of this tool material are listed in Table 1. Micro-EDM was applied to fabricate micro-holes on the tool-chip contact zone using micro-EDM equipment (type: DZW-10) as shown in Fig. 1. The process parameters for the micro-holes were as follows: average voltage was 125 V, and capacitance was 4.45 nF.

Graphite with diameter of 1 μm was embedded into the micro-holes to form self-lubricating cemented carbide. The micrographs of the micro-holes on the carbide rake face embedded without and with graphite are exhibited in Fig. 2. The average diameter of the micro-hole was about 150 ± 10 μm, and the depth was about 200 ± 10 μm.

2.2 Cutting tests

Dry cutting tests were conducted on a CA6140 lathe equipped with a commercial tool holder having the following geometry: rake angle $\gamma_o = 8°$, clearance angle $\alpha_o = 8°$, inclination angle $\lambda_s = 2°$, and side cutting edge angle $k_r = 45°$. Cutting tools

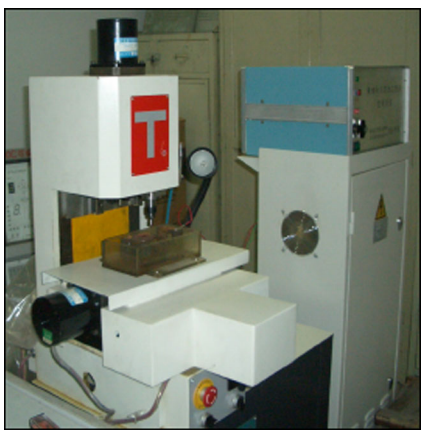

Fig. 1 Photo of the micro-EDM equipment

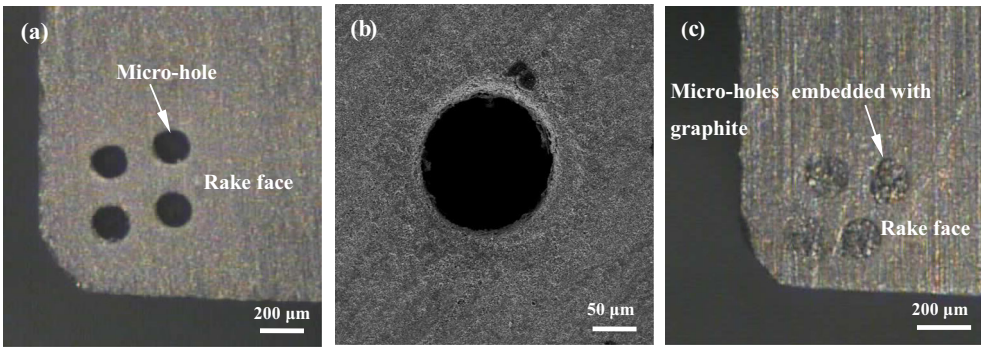

Fig. 2 Micrographs of the micro-holes on the carbide rake face. **a** Micro-holes filled without graphite. **b** Enlarge micrograph corresponding to **a**. **c** Micro-holes filled with graphite

were used with the cemented carbide tool embedded with graphite (ST) and the conventional one without micro-holes and graphite (CT) for comparison. The geometry of the inserts was of ISO SNGN150608. The workpiece material utilized was AISI 1045 hardened steel with a hardness of HRC 35–40. All tests were carried out with the cut depth a_p of 0.2 mm, feed rate f of 0.1 mm/r, cutting speed v of 60–180 m/min, and cutting time of 5 min.

Cutting temperature of chip was obtained by a TH5104R infrared thermal imaging system. Each test was replicated three times to ensure the reproducibility of test result. The wear properties of the cutting tools were investigated using scanning electron microscope (SEM) and energy dispersive X-ray analysis (EDX) to study the mechanism of the ST tool.

3 Results and discussion

3.1 Cutting temperature

The average value of the highest cutting temperatures during cutting process was obtained using the infrared thermal imaging system at 10 s intervals. Figure 3 illustrates the cutting temperature distribution of chip with ST tool in dry cutting hardened steels at speed of 140 m/min, and the maximum cutting temperature of chip under this cutting condition was about 510 ± 5 °C.

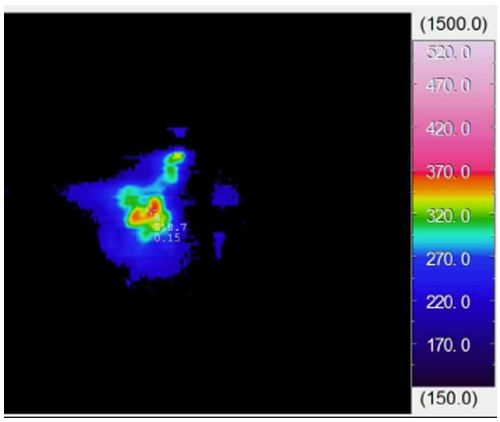

Fig. 3 Cutting temperature distribution of chip with ST tool in dry cutting hardened steels (a_p = 0.2 mm, f = 0.1 mm/r, v = 140 m/min)

Figure 4 shows the average cutting temperature of chip as a function of cutting speeds with the ST and CT tools. It was obvious that the cutting temperature increased with the increasing cutting speed, and it was higher than 500 °C when the cutting speed was above 140 m/min for the two kinds of tools. The cutting temperature of chip with the ST tool embedded with graphite was reduced by 15–20% in comparison with that of the CT one under the same cutting condition.

3.2 Tool wear on the rake face and flank face

Figure 5 exhibits the flank wear of the ST and CT tools in dry cutting of hardened steel at conditions of a_p = 0.2 mm, f = 0.1 mm/r, and cutting time = 5 min. It was indicated that the flank wear of two kinds of tools increased with the growth of cutting speed, and the ST cutting tool possessed the smaller flank wear compared with the CT carbide tools. It meant that the ST tool had played a role in improving flank wear resistance during cutting process.

Wear morphology and composition analysis test on the tool face are usually conducted to compare the tribological properties of the tested tools. Figure 6 shows SEM micrograph of the worn tool face and the corresponding EDX composition analysis of the conventional CT tool. As shown in Fig. 6a, b, c, it was clearly evident that there existed serious abrasive wear on the rake face and flank face, which was characterized by mechanical plowing grooves in the direction of tool sliding against chip and workpiece. Significant adhesion wear could also be seen on the rake face, which was identified to be Fe element of chip by EDX composition analysis as shown in Fig. 6d, e. It was noted that the Fe element was stripped from the chip and transferred to the tool rake face, and then adhered to the tool rake face. The repeated adhesion and flaking of the chip to the tool could accelerate the friction and wear of the tool rake face.

Figure 7 illustrates SEM micrograph of the worn face and the corresponding EDX composition analysis on the worn surface of the ST tool after 5 min dry cutting at speed of 140 m/min. From Fig. 7a, b, and c, it was obvious that there existed plows and abrasive wear on the rake face and flank face, yet the tool wear for the ST tool was relatively mild compared to that of the CT tool under the same test condition. Figure 7d–g exhibits the

corresponding EDX composition analysis of point A–D in Fig. 7a, b. It indicated that there was adhesion wear on the rake face owing to high cutting temperature and severe friction. To better evaluate the mechanism of worn rake face, EDX maps of C and Fe element distributions on the tool rake surface are shown in Fig. 8. The analysis results indicated that graphite could be released from the micro-holes and unevenly smeared on the rake face. The graphite film was propitious to alleviate the adhesion and abrasive wear on the rake face of the ST tool. Moreover, it could be seen that the Fe element of chip was entrapped in the micro-holes, and the micro-holes could act as storage for chip powder to reduce the abrasive wear on the rake face.

4 Discussion

4.1 Cutting temperature distribution

The temperature rise in cutting process is mainly composed of three parts [29]: the chip elastic and plastic deformation on the shear plane, the friction at the tool-chip interface, and the friction at tool-workpiece interface. The cutting thermal created on the shear plane transfers into the chip and then through the tool-chip interface into the tool substrate, hence the cutting heat produced on the shear plane influences the temperature rise of both tool and chip. It is usually considered that the temperature rise caused by tool-workpiece friction on the flank face is too small to be ignored for one new tool with smaller tool radius. Therefore, the cutting heat distribution produced in cutting process can be simplified representation in Fig. 9. The average value of maximum cutting temperature on the rake face is applied to evaluate cutting temperature owing to the complexity of cutting process, and it consists of the heat caused by chip deformation on the shear plane and the heat caused by chip friction on the rake face [29–31]. As a result, the cutting temperature rise can be expressed as follows:

$$\overline{\theta}_{\mathrm{t}} = \overline{\theta}_{\mathrm{s}} + \overline{\theta}_{\mathrm{f}} \tag{1}$$

$$\overline{\theta}_{\mathrm{tt}} = \overline{\theta}_{ft} \tag{2}$$

where $\overline{\theta}_{\mathrm{t}}$ and $\overline{\theta}_{\mathrm{tt}}$ are the average cutting temperatures of chip and tool respectively, $\overline{\theta}_{\mathrm{s}}$ is the average temperature rise of chip due to chip deformation on the shear plane, $\overline{\theta}_{\mathrm{f}}$ and $\overline{\theta}_{ft}$ are the average temperature rises of chip and tool owing to the tool-chip friction on the rake face.

4.2 Cutting temperature distribution on the shear plane

The power consumption of chip per unit time on the shear plane can be obtained by [29]:

$$U_s = F_s v_s \tag{3}$$

$$vs = \frac{v\cos\gamma_o}{\cos(\phi - \gamma_o)} \tag{4}$$

where u_{s} is the consumed power per unit time on the shear plane, F_{s} is the shear force of chip, ν_{s} is the shear speed, ν is the cutting speed, ϕ is the shear angle, and γ_{o} is the rake angle.

The heat flux on the shear plane can be indicated by:

$$q_s = \frac{U_s}{a_{\mathrm{c}} a_{\mathrm{w}} \csc\phi} = \frac{F_s v_s}{a_{\mathrm{c}} a_{\mathrm{w}}} \sin\phi \tag{5}$$

As shown in Fig. 9, $R_1 q_{\mathrm{s}}$ is the heat transfer into chip on the shear plane, $(1\text{-}R_1)q_{\mathrm{s}}$ is the heat flow into workpiece, a_{w} is the cut depth, and a_{c} is the cut width. Then, the average temperature of chip on the shear plane can be expressed as follows:

$$\begin{aligned} \overline{\theta}_s = \quad \theta_0 + \frac{R_1 q_s}{c_1 \rho_1 \upsilon \sin\phi} = \quad \theta_0 + \frac{R_1}{c_1 \rho_1 \upsilon \sin\phi} \frac{F_s v_s}{a_c a_w} \sin\phi \\ \theta_0 + \frac{R_1}{c_1 \rho_1 \upsilon a_{\mathrm{c}} a_w} \frac{v\cos\gamma_o}{\cos(\phi - \gamma_o)} \frac{\tau_{\mathrm{s}} a_{\mathrm{c}} a_{\mathrm{w}}}{\sin\phi} = \theta_0 + \frac{R_1 \tau_s \cos\gamma_o}{c_1 \rho_1 \cos(\phi - \gamma_0)\sin\phi} = \theta_0 + \frac{R_1 \tau_s \cos\gamma_o}{c_1 \rho_1 (\sin(2\phi - \gamma_0) + \sin\gamma_0)} \end{aligned} \tag{6}$$

where R_1 is the ratio of heat flow into the chip to the total heat on the shear plane, c_1 is the chip heat capacity at temperature of $\left(\theta_0 + \overline{\theta}_s\right)/2$, ρ_1 is the workpiece density, τ_{s} is the shear strength of the workpiece, and θ_0 is the ambient temperature.

4.3 Cutting temperature distribution on the rake face

As shown in Fig. 9, q_{r} is heat flux at the tool-chip interface, and it is expressed by [31]:

$$q_r = \frac{F_{\mathrm{f}} v_{\mathrm{ch}}}{l_{\mathrm{f}} a_{\mathrm{w}}} \tag{7}$$

where v_{ch} can be obtained by $v_{\mathrm{ch}} = v/\xi$, and F_{f} is the friction force on the rake face, v_{ch} is the chip flow speed, l_{f} is the actual contact length between tool and chip, and ξ is the chip deformation coefficient.

Then, friction power per unit u_{r} can be given by:

$$u_{\mathrm{r}} = \frac{F_{\mathrm{f}} v_{\mathrm{ch}}}{v a_{\mathrm{c}} a_{\mathrm{w}}} \tag{8}$$

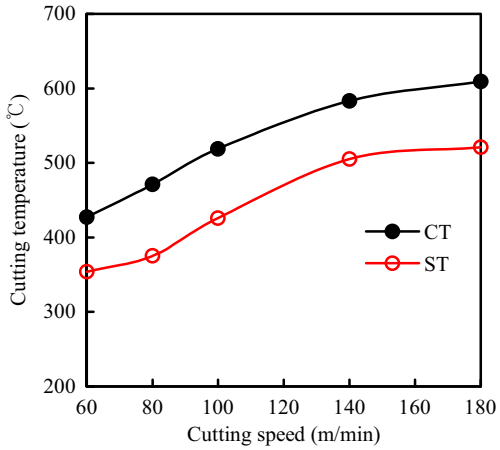

Fig. 4 Cutting temperature of CT and ST tool in dry cutting of hardened steel at different cutting speeds (a_p = 0.2 mm, f = 0.1 mm/r, cutting time 5 min)

Applying Eq. (8) to satisfy (7), it is obtained as:

$$q_r = \frac{u_r v a_c}{l_f} \tag{9}$$

From Fig. 9, the tool substrate is so large that the part B could be assumed to move to part A to form an approximate semi-infinite body surface. Then, the cutting heat conduction could be simplified to move on the semi-infinite body as shown in Fig. 10. $R_2 q_r$ is the heat flow into chip in the tool-chip contact area, and R_2 is the ratio of heat flow into the chip to the total heat generated by the tool-chip friction. The average temperature rise at the tool-chip interface caused by friction can be calculated by:

$$\overline{\theta}_f = 0.7524 \frac{ql}{k\sqrt{L}} \tag{10}$$

On the basis of Eqs. (7)–(9), Eq. (10) can be expressed as follows:

$$\overline{\theta}_f = \frac{0.7524 R_2 q_r^{\frac{lf}{2}}}{k_2 \sqrt{l_2}} \tag{11}$$

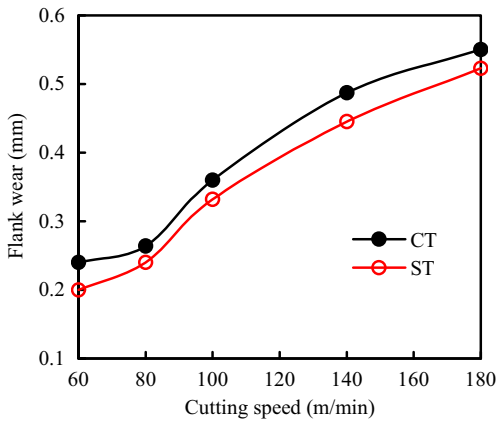

Fig. 5 Flank wear of CT and ST tools in dry cutting of hardened steel (a_p = 0.2 mm, f = 0.1 mm/r, cutting time 5 min)

$$L_2 = \frac{v_{ch}(l_f/2)}{2\omega_2} \tag{12}$$

$$\omega_2 = \frac{k_2}{c_2 \rho_2} \tag{13}$$

where k_2 is the chip thermal diffusivity coefficient at temperature of $(2\overline{\theta}_s + \overline{\theta}_f)/2$, L_2 is the heat source width, w_2 is the chip thermal diffusivity at temperature of $(2\overline{\theta}_s + \overline{\theta}_f)/2$, ρ_2 and c_2 are the chip density and heat capacity respectively at temperature of $(2\overline{\theta}_s + \overline{\theta}_f)/2$.

Then, the average temperature rise of chip and tool caused by tool-chip friction can be determined as follows:

$$\overline{\theta}_f = \frac{0.7524\frac{l_f}{2}}{k_2\sqrt{L_2}} R_2 q_r = 0.7524 R_2 \overline{\tau}_c \sqrt{\frac{k_2 v a_w l_f}{c_2 \rho_2 \xi}} \tag{14}$$

$$\overline{\theta}_{fi} = 0.7524(1-R_2)\overline{\tau}_c \sqrt{\frac{k_2 v a_w l_f}{c_2 \rho_2 \xi}} \tag{15}$$

where ξ is the deformation coefficient of the chip and $\overline{\tau}_c$ is the average shear stress at the tool-chip interface, which can be expressed by:

$$\overline{\tau}_c = k\tau_c + (1-k)\tau_f \tag{16}$$

where k is the proportion between real contact area and appearance contact area, τ_c is the shear stress of chip material, and τ_f is the shear stress of lubricating film formed on the rake face.

Therefore, the average cutting temperature of chip and tool can be obtained from the formula as follows:

$$\overline{\theta}_t = \overline{\theta}_s + \overline{\theta}_f = \overline{\theta}_0 + \frac{R_1 \tau_s \cos\gamma_o}{c_1 \rho_1 (\sin(2\phi - \gamma_0) + \sin\gamma_0)} + 0.7524 R_2 \overline{\tau}_c \sqrt{\frac{k_2 v a_w l_f}{c_2 \rho_2 \zeta}} \tag{17}$$

$$\overline{\theta}_{tt} = \overline{\theta}_s + \overline{\theta}_{fi} = \overline{\theta}_0 + \frac{R_1 \tau_s \cos\gamma_o}{c_1 \rho_1 (\sin(2\phi - \gamma_0) + \sin\gamma_0)} + 0.7524(1-R_2)\overline{\tau}_c \sqrt{\frac{k_2 v a_w l_f}{c_2 \rho_2 \zeta}} \tag{18}$$

As shown in Eqs. (17)–(18), the cutting parameters such as cut width α_w, cutting speed v, rake angle γ_o, chip heat capacity c_1, workpiece density ρ_1, ambient temperature θ_0, chip density ρ_2, and heat capacity c_2 have been given in practical cutting. The workpiece shear stress τ_s, the shear angle ϕ, the ratio of heat flow R_1, and the ratio of heat flow R_2 keep constant under the same cutting conditions [29–31]. According to Eqs. (17)–(18), the cutting temperature variation of chip and

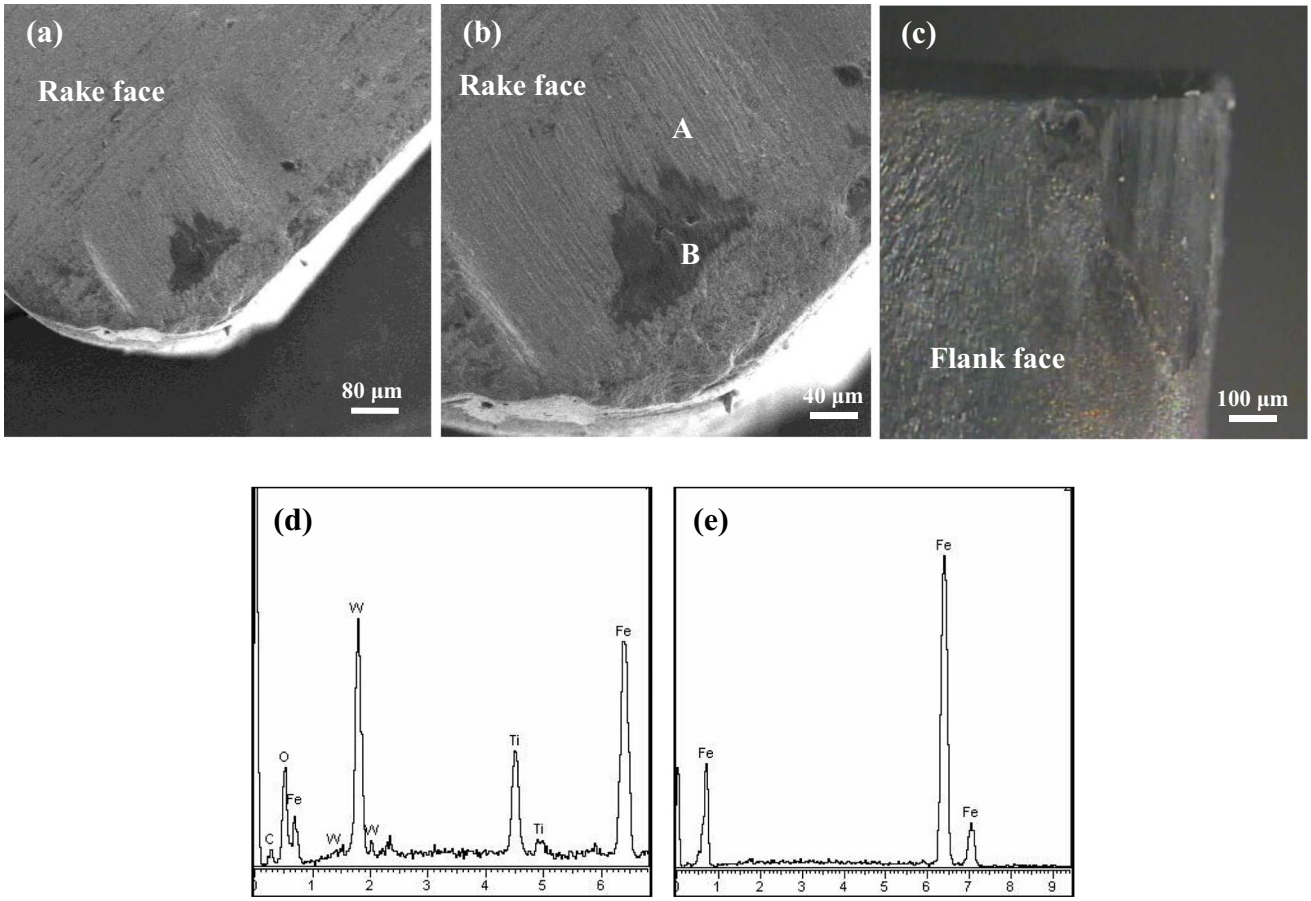

Fig. 6 SEM micrographs and EDX composition analysis of the CT tool surface at speed of 140 m/min. **a** SEM micrograph of the worn rake face. **b** Enlarge micrograph corresponding to **a**. **c** SEM micrograph of the worn flank face. **d** and **e** Corresponding EDX composition analysis of point A and B in **b**

tool keep in accordance with the average shear stress $\overline{\tau}_c$ and actual contact length l_f at the tool-chip interface.

As an extensively applied solid lubricant in the industry, graphite owns much lower shear stress compared with that of chip. Due to the frictional extrusion of chip and high cutting temperature in dry cutting process, the graphite solid lubricants may be released from the micro-holes and smeared unevenly on the tool face. Then, a discontinuous and/or continuous graphite film may gradually create at the tool-chip interface, and this is in accordance with the SEM and EDX analysis results as shown in Figs. 7 and 8. Therefore, the friction and wear condition at the tool-chip interface is changed from dry friction to boundary lubrication, the tool substrate carries the load, the friction and wear behavior occurs on the lubricating film between tool and chip, and results in the self-lubrication performance. If the proportion k is about 80%, the portion of contact area covered with graphite is about 20%. Because of the existence of graphite lubricating film at the tool-chip interface, the average shear stress $\overline{\tau}_c$ will be decreased by 20% from Eq. (16). Therefore, the average temperature rise of chip and tool caused by tool-chip friction will be reduced by about 20% according to Eqs. (17)–(18).

In addition, the reduction of average shear stress $\overline{\tau}_c$ can influence shear angle and cutting temperature on the shear plane by reducing the friction angle β [29]. On the basis of Lee and Shaffer shear angle formula ($\phi + \beta - \gamma_o = C$) [30], the reduced friction angle β makes for the increase of shear angle ϕ, which is beneficial to reduce the cutting temperature of the chip and tool according to Eq. (16)–(17).

Moreover, the micro-holes at the tool-chip interface can reduce the actual contact length l_f as shown in Fig. 9, and then the actual tool-chip contact length l_f can be calculated as:

$$l_f = l_a - nd \tag{19}$$

where d is the diameter of the micro-hole, l_a is the theoretical contact length, and n is the number of the micro-holes at the tool-chip interface.

If the tool-chip contact length is 1.0 mm, and there are two micro-holes with diameter of 0.15 mm at the tool-chip interface, the actual tool-chip contact length l_f will be reduced by 30% (see Fig. 9). Then, the average temperature rise of chip and tool caused by tool-chip friction will be reduced by 16% according to Eqs. (16)–(17). At

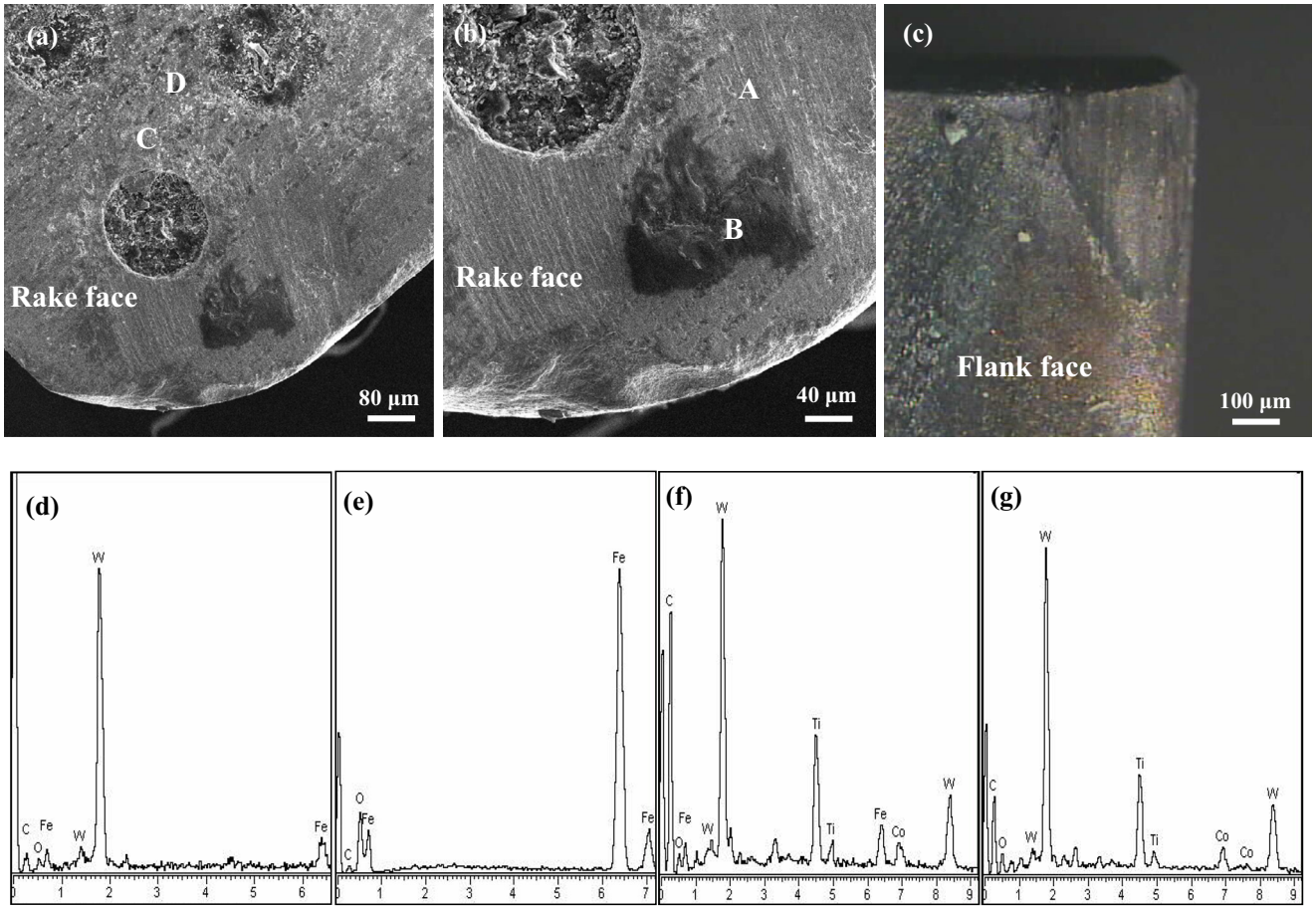

Fig. 7 SEM micrographs and EDX composition analysis of the ST tool surface after 5 min dry cutting at speed of 140 m/min. **a** SEM micrograph of the worn rake face. **b** Enlarge micrograph corresponding to **a**. **c** SEM micrograph of the worn flank face. **d**, **e**, **f**, and **g** Corresponding EDX composition analysis of point A, B, C, and D in **a** and **b**

the same time, the micro-holes can store more graphite and entrap chip debris, which are also helpful to reduce the friction and wear on the rake face.

At the same time, owing to the higher thermal conductivity (120 W/(mK)) [19], the graphite film at the tool-chip interface contributes to the reduction of cutting temperature of chip. Therefore, the ST tool embedded with graphite can effectively reduce the cutting temperature of chip and tool wear, and these are in line with the test results in Figs. 4 and 5.

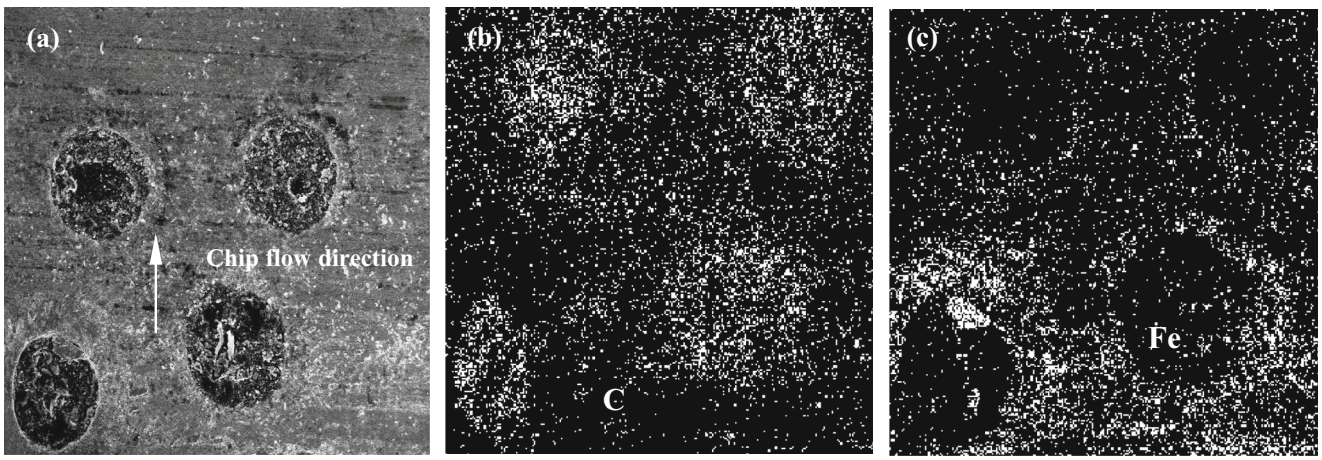

Fig. 8 Micrographs and EDX maps analysis of the ST rake surface tool after 5 min dry cutting at speed of 140 m/min. **a** SEM micrograph of the worn rake face. **b** and **c** Corresponding EDX maps of C and Fe element distributions in **a**

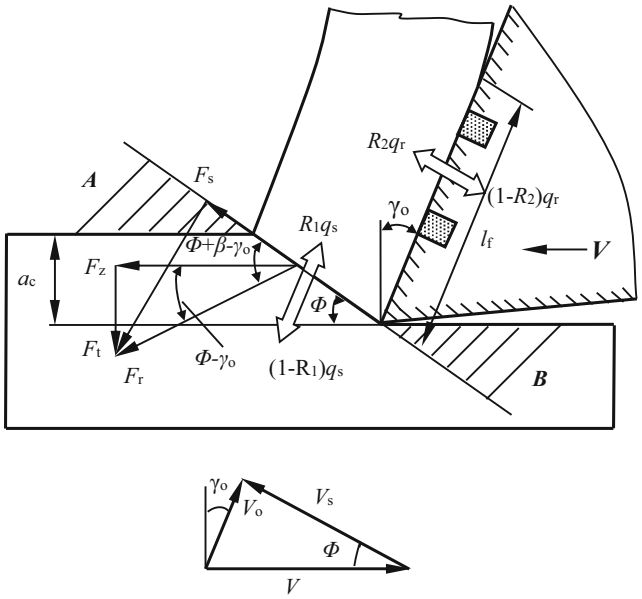

Fig. 9 Schematic diagram of heat distribution in orthogonal cutting

5 Conclusions

Textured micro-holes were fabricated using micro-EDM on the rake face of cemented carbide inserts, and graphite was embedded into the micro-holes to form self-lubricating tool. Dry cutting tests on hardened steel were carried out with the ST tool and CT one. The cutting temperature of chip and tool wear were investigated and compared. Through test results and cutting temperature theoretical analysis, the following conclusions were obtained:

1. The cutting temperature of the carbide tool embedded with graphite (ST) was lower by 15–20% than that of the conventional carbide tool (CT).
2. The tool wear of both rake face and flank face for the ST tool were smaller and milder than that of the CT one. The flank face revealed serious abrasive wear, while rake face exhibited abrasive wear and adhesion wear.
3. The primary mechanisms responsible for the reduced cutting temperature are put forward: first, owing to high cutting temperature and chip friction, graphite may be released from the micro-holes, and formed a thin discontinuous lubricating film at the tool-chip interface, which is beneficial to decrease the temperature of chip and tool caused by tool-chip friction and chip deformation. The second one is attributed to the reduced actual contact length at the tool-chip interface due to the micro-holes, which is propitious to lower the temperature of chip and tool caused by tool-chip friction, supply more graphite, and store chip debris. The decreased cutting temperature contributes to reducing carbide tool wear.

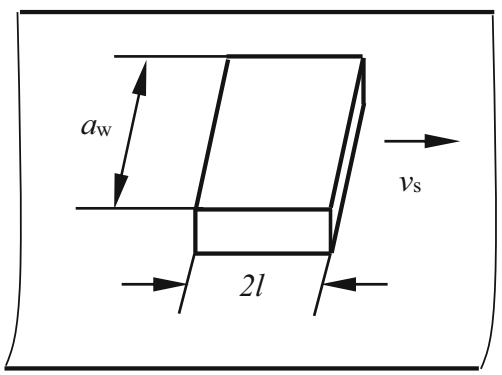

Fig. 10 Schematic of the heat conduction on semi-infinite body

Acknowledgements This work was supported by the "Natural Science Funds of Shandong Province (ZR2016EEB39)", "Scientific Research Planning Project of Shandong Province (J16LB02)", "China Postdoctoral Science Foundation (2016M592181)", "Postdoctoral Innovative Projects of Shandong Province (201603028)", and "Scientific Research Foundation of Jining University (2016BSZX04)".

References

1. Ai X (2004) High speed machining technology. National Defense Industry Press, Beijing
2. Serdyuk YD, Semizhon OA, Prokopiv NM, Petasyuk GA, Kharchenko OV, Mel'chuk TV (2011) The influence of thermal compression treatment parameters on quality characteristics and wear mechanisms of T5K10 carbide inserts in rough turning. J Superhard Mater 33:120–128
3. Özbek NA, Çiçek A, Gülesin M, Özbek O (2014) Investigation of the effects of cryogenic treatment applied at different holding times to cemented carbide inserts on tool wear. Int J Mach Tools Manuf 86:34–43
4. Ahmet M, Ihsan K (2014) Machinability of a Ti-6Al-4V alloy with cryogenically treated cemented carbide tools. Mater Technol 48: 577–580
5. Sahin Y, Sur G (2004) The effect of Al_2O_3, TiN, and Ti (C,N) based CVD coatings on tool wear in machining metal matrix composites. Surf Coat Technol 179:349–355
6. Dos Santos JABO, Sales WF, Santos SC, Machado AR, da Silva MB, Bonney J, Ezugwu EO (2007) Tribological evaluation of TiN and TiAlN coated PM-HSS gear cutter when machining 19MnCr5 steel. Int J Adv Manuf Technol 31:629–637
7. Astrand M, Selinder TI, Fietzke F, Klostermann H (2004) PVD-Al_2O_3-coated cemented carbide cutting tools. Surf Coat Technol 188-189:186–192
8. Rivero A, Aramendi G, Herranz S, de Lacalle LNL (2006) An experimental investigation of the effect of coatings and cutting parameters on the dry drilling performance of aluminium alloys. Int J Adv Manuf Technol 28:1–11
9. Rech J, Kusiak A, Battaglia JL (2004) Tribological and thermal functions of cutting tool coatings. Surf Coat Technol 186:364–371
10. Deng JX, Song WL, Zhang H, Zhao JL (2008) Performance of PVD Ti-MoS_2/Zr coated carbide in cutting processes. Int J Mach Tools Manuf 48:1546–1552
11. Renevier NM, Hamphire J, Fox VC (2001) Advantages of using self-lubricating, hard, wear-resistant MoS_2-based coatings. Surf Coat Technol 142-144:67–77
12. Renevier NM, Oosterling H, Kőnig U, Dautzenberg H, Kim BJ, Geppert L, Koopmans FGM, Leopold J (2003) Performance and

limitations of MoS_2/Ti composite coated inserts. Surf Coat Technol 172:13–23
13. Renevier NM, Fox VC, Teer DG, Hampshire J (2000) Performance of low friction MoS_2/titanium composite coatings used in forming applications. Mater Des 21:337–343
14. Tsao CC (2007) An experiment study of hard coating and cutting fluid effect in milling aluminum alloy. Int J Adv Manuf Technol 32: 885–891
15. Abdel-Aal HA, Nouari M, El Mansori M, Ginting A (2008) Conceptual tribo-energetic analysis of cutting tool protective coating delamination in dry cutting of hard-to-cut aero engine alloys. Int J Adv Manuf Technol 36:213–225
16. Borghi A, Gualtieri E, Marchetto D, Moretti L, Valeri S (2008) Tribological effects of surface texturing on nitriding steel for high-performance engine applications. Wear 265:046–1051
17. Song WL, Deng JX, Zhang H, Yan P (2010) Study on cutting forces and experiment of MoS_2/Zr coated cemented carbide tool. Int J Adv Manuf Technol 2010.08(49):903–909
18. Song WL, Deng JX, Zhang H, Yan P (2011) Cutting performance of cemented-carbides-based self-lubricated tool embedded with different solid lubricants. Int J Adv Manuf Technol 52:477–485
19. Shi MS (2000) Solid lubricating materials. China Chemical Industry Press, Beijing
20. Lei S, Devarajan S, Chang ZH (2009) A study of micropool lubricated cutting tool in machining of mild steel. J Mater Process Technol 209:1612–1620
21. Sugihara T, Enomoto T (2009) Development of a cutting tool with a nano/micro-textured surface improvement of anti-adhesive effect by considering the texture patterns. Precis Eng 33(4):425–429
22. Hu TC, Zhang YS, Hu LT (2012) Tribological investigation of MoS_2 coatings deposited on the laser textured surface. Wear 278-279:77–82
23. Obikawa T, Kamio A, Takaoka H, Osada A (2011) Micro-texture at the coated tool face for high performance cutting. Int J Mach Tools Manuf 51:966–972
24. Deng JX, Wu Z, Lian YS, Qi T, Cheng J (2012) Performance of carbide tools with textured rake face filled with solid lubricants in dry cutting processes. J Refract Met Hard Mater 30:164–172
25. Deng JX, Lian YS, Wu Z, Xing YQ (2013) Performance of femtosecond laser-textured cutting tools deposited with WS_2 solid lubricant coatings. Surf Coat Technol 222:135–143
26. Xing YQ, Deng JX, Wang XS, Meng R (2015) Effect of laser surface textures combined with multi-solid lubricant coatings on the tribological properties of Al_2O_3/TiC ceramic. Wear 342-343: 1–12
27. Zhang KD, Deng JX, Sun JL, Jiang C, Liu YY, Chen S (2015) Effect of micro/nano-scale textures on anti-adhesive wear properties of WC/Co-based TiAlN coated tools in AISI 316 austenitic stainless steel cutting. Appl Surf Sci 355:602–614
28. Zhang KD, Deng JX, Xing YQ, Li SP, Gao HH (2015) Department effect of microscale texture on cutting performance of WC/Co-based TiAlN coated tools under different lubrication conditions. Appl Surf Sci 326:107–118
29. Usui E (1982) Mechanical metal processing. China Machine Press, Beijing
30. Chen RY (1993) Metal-cutting principles. China Machine Press, Beijing
31. Nakayama K (1985) Principle of metal cutting. China Machine Press, Beijing